Cumhuriyet Sci. J., 46(4) (2025) 791-804
DOI: https://doi.org/10.17776/csj.1685750

Cumhuriyet Science Journal

| csj.cumhuriyet.edu.tr | Founded: 2002 ISSN: 2587-2680 e-ISSN: 2587-246X Publisher: Sivas Cumhuriyet University

Improvement Of Ti6Al4V Alloy Surface Via Micro Arc Oxidation Treatment And UV-Assisted Thread-Like Silver Deposition

Kadir Ünlüses[1, a,*], Kürşad Oğuz Oskay[1,b], Ebru Yabaş[2,3,c], Mehmet Şimşir[3,1,d]

[1]Department of Metallurgy and Material, Faculty of Engineering, Sivas Cumhuriyet University, Sivas, Türkiye
[2]Advanced Technology Application and Research Center, Sivas Cumhuriyet University, Sivas, Türkiye
[3]ESTAŞ Eksantrik Sanayi ve Ticaret A.Ş., Sivas, Türkiye
*Corresponding author

Research Article

History
Received: 29/04/2025
Accepted: 20/10/2025

ABSTRACT

Titanium and titanium alloys are widely used as biomaterials. However, in order to ensure a permanent integration between the implant and the surrounding tissue, the surface properties of these materials need to be improved. Although various surface treatment methods exist, micro-arc oxidation (MAO) is among the most commonly used techniques. In this study, the MAO process was applied to Ti6Al4V alloy using an electrolyte composed of 11 g trisodium phosphate ($Na_3PO_4 \cdot 12H_2O$), 2 g calcium acetate hydrate ($(CH_3COO)_2Ca \cdot H_2O$), and varying amounts of EDTA-Na_2. EDTA-Na_2 addition enhanced calcium incorporation, controlled pore size, and altered wettability of MAO coatings. Varying EDTA-Na_2 concentrations produced different pore diameters and promoted rutile phase formation, resulting in mixed anatase–rutile surfaces. The porous structure obtained after the MAO process increased the surface roughness.Following MAO treatment, silver was deposited by UV irradiation using a custom-made photoreactor, with solutions containing varying concentrations of $AgNO_3$ and glucose monohydrate. The resulting silver structures were found to have a thread-like morphology. Additionally, ion release analyses showed that silver ions were released into simulated body fluid (SBF) over five days. This indicates it has the potential for long-term antibacterial activity. The combined photoreactor–UV approach provides a low-cost, room-temperature, and environmentally friendly method for antibacterial functionalization of the Ti6Al4V surface. To the best of our knowledge, the deposition of silver onto the MAO-treated Ti6Al4V surface with the UV irradiation method has been reported for the first time in the literature. Moreover, thread-like silver structures have not been encountered in the literature.

Keywords: Micro-Arc oxidation, UV irradiation method, Silver deposition, Silver nanostructure

[a] kadirunluses@gmail.com https://orcid.org/0009-0004-8170-193X
[b] koskay@cumhuriyet.edu.tr https://orcid.org/0000-0003-4026-867X
[c] eyabas@cumhuriyet.edu.tr https://orcid.org/0000-0001-7163-3057
[d] msimsir@cumhuriyet.edu.tr https://orcid.org/0000-0002-8895-7821

Introduction

Biomaterials are artificial materials found in nature or produced synthetically. For the making of implants, these materials are used to replace biological structures that no longer exist or have been damaged and to provide function and form. Thereby, biomaterials help improve the quality and duration of people's lives, and the field of biomaterials has rapidly developed to meet the demands of an aging population. Biomaterials like artificial stents in veins, artificial heart valves, shoulder replacement implants, knee joints, elbows, ears, orodental structures, and hip joints are used in the human body [1]. A large number of titanium alloys are commercially available these days, but unalloyed titanium and the Ti6Al4V alloy are widely used in biomedical applications. Mostly, unalloyed titanium is utilised for the production of dental implants. The most popular biomaterial among titanium alloys is Ti6Al4V alloy, and more than 50% of the world's titanium production is produced in this alloy since Ti6Al4V has high strength, low density, and good chemical resistance. Also, contrary to other metallic materials (cobalt–chromium alloys and stainless steels), Ti6Al4V has a closer modulus of bone elasticity, making Ti6Al4V alloy a convenient biomaterial [2-4].

An ideal implant should be similar to natural bone in terms of its structural, mechanical, and biological properties. In titanium-based bone implants, the porous structure of the surface and chemical composition of the material are important factors in promoting bone regeneration. Surface treatments are required to advance the structural and biological characteristics of titanium alloys. Among surface modification methods, micro-arc oxidation (MAO) for biomedical applications has the potential to make the surface a biocompatible and bioactive coating [5].

The micro-arc oxidation (MAO) process is a surface modification technique that has been developed in recent years. A porous, comparably rough, and very tightly adherent titanium oxide layer on the titanium surface is obtained through the MAO process [6,7]. The MAO process is performed in an electrolytic solution containing modifying elements in the form of dissolved salts (e.g., calcium and phosphorus), and these elements incorporate into the formed coating. C and P ions in the coating layer can increase the bonding between the implants and the bone and usually appear to induce bone-like apatite in simulated body fluid (SBF) [8]. The MAO process consists of three stages. At the first stage of the coating process, in a region of low electrical conductivity, after losing dielectric stability, many microdischarge channels form on the surface. Thus, these micro sparks move on the surface and can be observed. Micro sparks cause a local temperature rise between 2000 and 10,000 K in the discharge channels due to electron collisions. Anionic compounds in the electrolyte are attracted to the discharge channels due to the presence of the electric field. Titanium melts due to the increase in temperature, and it moves into the discharge channels. As a result of this process, plasma channels form on the surface. At the second stage of the process, plasma chemical reactions occur in the plasma channels, and the pressure in the channels improves. As the current is increased, the microdischarge channels gradually enlarge to reduce the pressure. In this way, the high current flow makes the surface of the coating more porous. When the applied voltage increases, the electrical resistance of the solution declines, and a thicker coating occurs. The reason for this is that as the current density increases, the discharge channels also increase [9–11]. After micro arc oxidation process, the coating has superior mechanical properties when compared with those fabricated by anodic oxidation [12]. The MAO process can be carried out in an acidic electrolyte or an alkaline electrolyte. This process can be carried out using the galvanostatic or potentiostatic mode. Time, voltage, current density, electrolyte composition, and temperature all play crucial roles in tailoring the implant surface's tribological, chemical, structural, and biocompatible characteristics. The most important criterion is additives in alkaline or acidic electrolytes [13].

However, one of the most important problems is bacterial colonization after implantation. Under body conditions, bacteria can proliferate around implants and can penetrate soft tissue. At this stage, bacterial infections occur and cause devastating complications and implant loss. However, it is possible to reduce or prevent bacterial colonization on implant surfaces by incorporating elements such as Ag, Cu, Zn into coating surfaces as an anti-bacterial agent [14].

Numerous techniques have been reported for depositing silver onto titanium and titanium alloys, including hydrothermal synthesis, sol–gel processing, impregnation, electrodeposition, photodeposition, and others. Among these methods, photodeposition is a basic method, and the content of silver is easily controlled at a safe range [15]. In the photoreduction method, different light sources such as UV LED, xenon lamp, and nanosecond laser can be used. $AgNO_3$ is the main material used for the synthesis of nano-silver. The wavelength of the source is an essential parameter to determine the shape of silver nanoparticles (AgNp). A small aspect ratio is obtained using a short irradiation wavelength. In addition, another important parameter affecting AgNP sizes is the liquid medium, whether or not surfactant is present, but the presence of surfactant terminates the formation of nanoparticles. The formation of nanoparticles is small in high surfactant concentration and is large in low surfactant concentration [16].

In this study, Trisodium phosphate dodecahydrate ($Na_3PO_4{\cdot}12H_2O$) as phosphorus (P) source, calcium acetate hydrate $(CH_3COO)_2Ca{\cdot}H_2O$ as calcium (Ca) source, and ethylene diamine tetraacetic acid disodium (EDTA-Na_2) as pore size controller were selected. The MAO process was conducted successfully. It was provided to add ions of Ca and P into the coating layer. A morphologically and chemically bone-like structure was obtained by creating a porous structure in the coating layer and adding Ca and P ions to the coating layer. The pore size, wettability, surface roughness, and chemical composition of the coating layer were changed after MAO treatment with EDTA-Na_2 addition into the electrolyte. The deposition of silver nano-structures onto the coating layer was successfully conducted using the ultraviolet (UV) irradiation method. Thus, the sample was given antibacterial properties. The prediction of silver nanostructures (AgNs) using UV light on the coating layer obtained by the MAO method is the first in the literature.

Experimental

MAO Process

In this chapter, Ti6Al4V (ELI 23) was used as a substrate. Pipe-shaped Ti6Al4V alloy was cut into disc-shaped samples using CNC machines. The diameter of the samples is 15 mm, and the thickness is 2 mm. Before the MAO process, the samples were cleaned in an ultrasonic-assisted caustic bath to remove grease residues, followed by rinsing in a hot deionized water bath. After degreasing, the native oxide layer was removed with a commercial acidic solution, thereby activating the sample surface for the subsequent MAO treatment. A schematic diagram for the MAO process is demonstrated in Fig. 1. Activated samples are used as anode, and a titanium sheet is used as cathode. The electrolytes were prepared by mixing various amounts of $Na_3PO_4{\cdot}12H_2O$ and $(CH_3COO)_2Ca{\cdot}H_2O$ with/without EDTA-Na_2. A DC power of 355 V was applied to all specimens for 330 sec. After the MAO process, samples are washed with a compressed vapour machine containing deionised water and air dried. The MAO process was conducted in alkaline electrolytes, and the experimental conditions are summarized in Table 1.

Table 1. The composition of electrolytes

Electrolyte Type	Sample Name	$Na_3PO_4{\cdot}12H_2O$ (g/L)	$(CH_3COO)_2Ca{\cdot}H_2O$ (g/L)	EDTA-Na_2 (g/L)	pH
Alkaline	B1	11	2	0	12,2
	B2	11	2	5	11,9
	B3	11	2	7,5	9,1
	B4	11	2	9	8,1

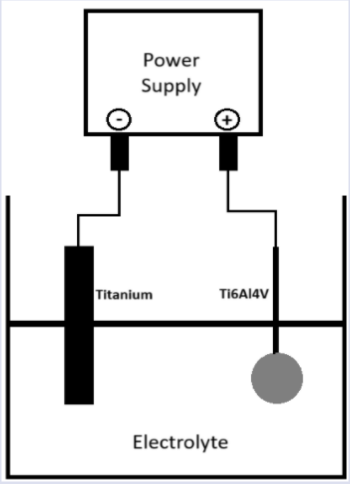

Figure 1. Schematic view of the MAO process.

Preparation of Silver Nanostructure Deposition with the UV Irradiation Method

To deposit silver nanostructures on an MAO-treated surface, the UV irradiation method that utilizes UV-A (365nm) lamps is selected. A photoreactor was designed using "SOLIDWORKS 3D" and manufactured to conduct this experiment.

Design and fabrication of the photoreactor device

The photoreactor consists of 3 main parts. The first is named "dark chamber" where we conducted the photochemical reduction experiments. The second one is "cover" to close around "dark chamber". The third one is "storage" where you can save the samples. This photoreactor provides a dark environment, so experiments were conducted in sunlight-free media. This photoreactor has 15 pieces of UV-A lamp (365nm) with 8W (7 pieces of lamp on top, 4 pieces of lamp on left side, and 4 pieces of lamp on right side) (max 120W), cooler fan to throw out warming air and thermometer to measure the heat of photoreactor. This photoreactor was manufactured using 430 stainless steel. The UV-A lamps were connected in series, allowing the desired power to be adjusted by switching the lamps on or off. The 3D model of the photoreactor is demonstrated in Fig 2.

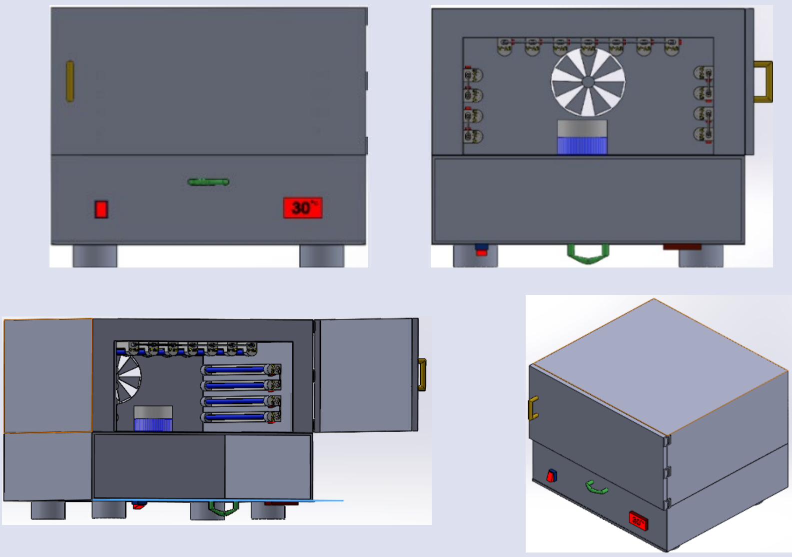

Figure 2. Appearance of the photoreactor from different aspects.

Silver nanostructure deposition

Ag deposition on the MAO-treated Ti6Al4V surface was performed using 120W UV-A lamp in the photoreactor. Two different solutions were prepared. One sample was selected after the MAO process for Ag deposition. As standard conditions, 100 mg silver nitrate ($AgNO_3$), 100 mg glucose monohydrate ($C_6H_{12}O_6 \cdot H_2O$), and 30 mL deionized water were mixed with a stirrer. The solution was placed right in the middle of "dark chamber" of the photoreactor, and the MAO-treated sample was placed into the solution. The distance between all lamps and the solution is 15 cm. This distance is a standard distance according to the literature. The photoreactor was operated, and the sample was irradiated for 1 hour with 120W UV-A lamp. After one hour of UV irradiation, the sample was kept in the solution for an additional hour. During this period, the AgNPs suspended in the solution settled and adhered to the surface. As an extreme condition, 1 g $AgNO_3$, 1 g $C_6H_{12}O_6 \cdot H_2O$, and 30 mL deionised water were mixed with a stirrer. This time, the solution was placed next to the left side, and the distance between the lamps on the left side and the solution was 1 cm. The sample was irradiated with a 120 W UV-A lamp for 3.5 hours. After the irradiation, it was kept in the solution for an additional hour. The second process was selected as extreme condition, and this condition is not in the literature. After the experiments, samples were taken out from solutions, washed with deionised water, and air dried. Silver nanostructure deposition parameters are summarized in Table 2.

Table 2. Silver nanostructure deposition process parameters.

Process Condition	$AgNO_3$ (g/L)	$C_6H_{12}O_6 \cdot H_2O$ (g/L)	Power (W)	Time (hour)	Distance (cm)
Standart	0,1	0,1	120	1	15
Extreme	1	1	120	3,5	1

Silver Release

The amount of released Ag from Ag deposited MAO surface was evaluated. 50 mL SBF solution was poured into a 100 mL glass bottle. For every sample, this preparation was repeated. Bottles were placed into an incubator and set at 36,5°C. Samples were immersed in glass bottles. After 1 day, 15 mL SBF solution was taken out from the bottles and poured into a Falcon tube. To prevent sticking of Ag ions to the Falcon tube, 1-2 drop of nitric acid was used and stored in a dark environment. This process was repeated on the 3rd and 5th days.

Sample Characterizations

To determine the chemical states of elements in MAO-treated samples, X-Ray Diffraction (XRD) (Rigaku MiniFlex) was performed with Cu Kα radiation (λ=1.5406 Å) at a scanning rate of 2°/min for 2θ ranging from 20° to 80°. For each sample, the average surface roughness (Ra) was measured using atomic force microscopy (AFM) (ZeeScope). Measured area is 3x2,5 µm, and 4x Na=0.1 objective is used. The surface wettability for MAO-treated samples was measured with a water contact angle goniometer operating in the sessile drop mode. In this method, a volume of 5 µL of water droplets was applied to the MAO-treated samples to measure the contact angle. The surface morphologies of the MAO-treated samples were examined with a scanning electron microscope (SEM) (TESCAN MIRA3). The elemental composition of each sample surface was analysed with an energy dispersive spectrometer (EDS) by using the area scanning mode. The average pore size was calculated using "ImageJ" application. The concentrations of Ag ions in SBF solutions were measured by inductively coupled plasma mass spectroscopy (ICP-MS) (Thermo iCAP Q)

Results and Discussion

SEM Analysis

SEM images show the surface morphology of samples (B1, B2, B3, and B4) after the MAO process in Fig. 3. It can be seen that the coating surface is porous, displaying the characteristic features of the MAO process. During the MAO process, due to the strong interaction between the substrate and the electrolyte in the discharge region, these pores are referred to as micro-discharge channels. In Fig. 3, it can be seen that sample B1 exhibits homogenously distributed pores and almost all of these pores are spherical as shape. With the addition of EDTA-Na_2, the pore characteristics changed (B2, B3, and B4). The sphericity of some pores is impaired. The reason for this is that some discharge channels become interconnected during the MAO process, leading to the formation of larger discharge channels. This phenomenon is referred to as "pore coalescence" in the literature. Around some pores, there is the non-porous area marked as a circle in Fig. 3. In a study conducted in the literature, it was observed that there were porous structures within the coating when the cross-sectional images were examined after the MAO process [17]. Therefore, it is assumed that beneath these non-porous regions, small micropores exist and are sealed by molten oxide. Consequently, the pore size distribution becomes more heterogeneous.

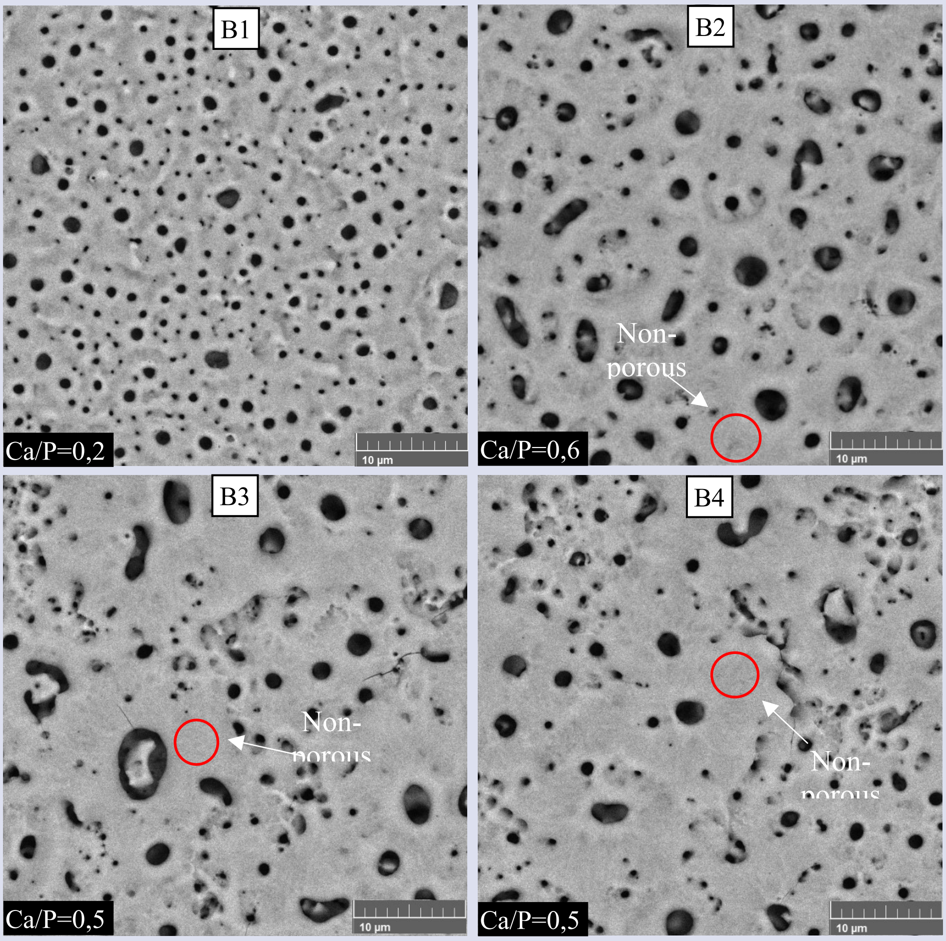

Figure 3. B1, B2, B3, and B4 SEM images after MAO treatment.

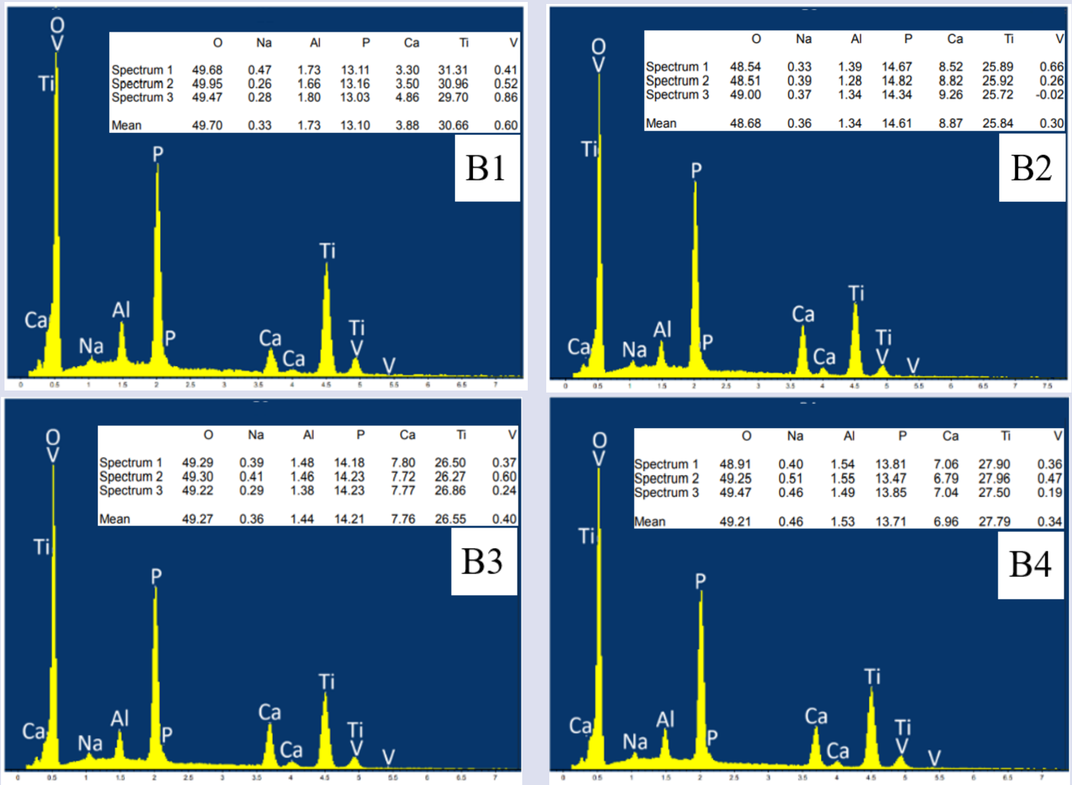

Figure 4. SEM-EDS analysis of B1, B2, B3, and B4 samples after MAO treatment.

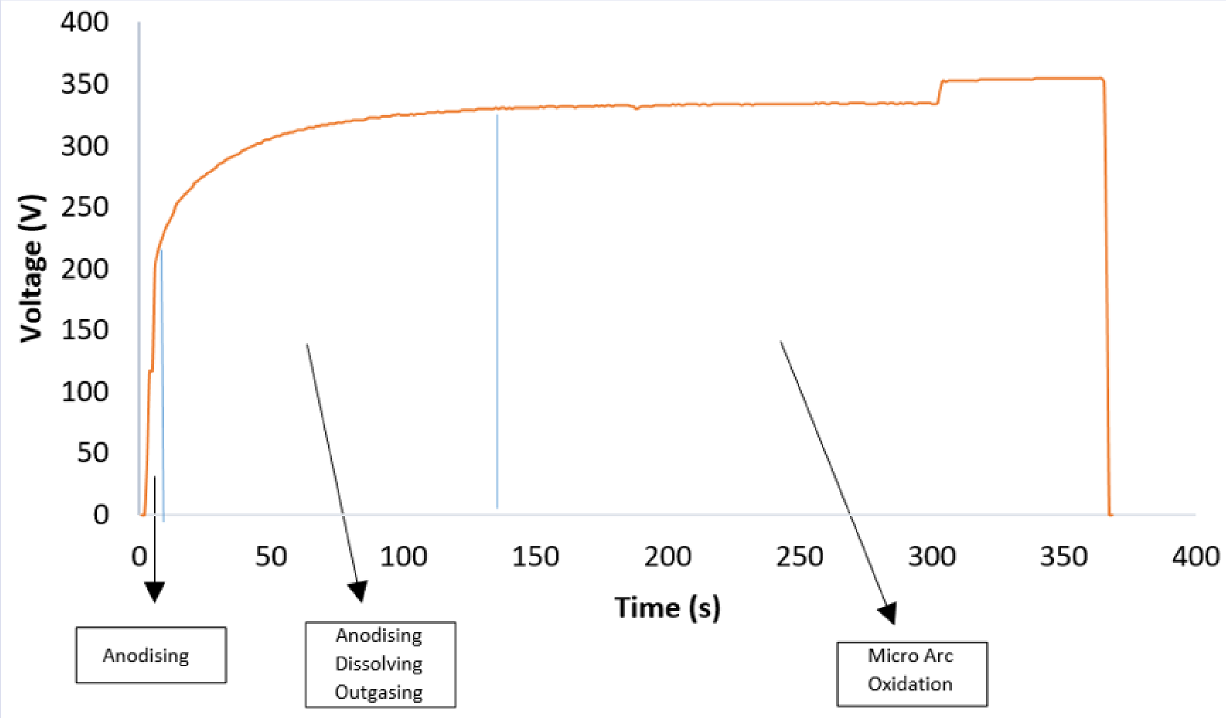

Figure 5. Voltage-time curve of the MAO process.

Fig. 4 shows the EDS result of B1, B2, B3, and B4 after MAO treatment. EDS shows that the surfaces of MAO-treated samples are composed of Ti, Ca, P, Al, O, Na, and V elements. The results confirmed that calcium and phosphorus from the electrolyte were effectively incorporated into the MAO coatings. Ca and P elements in B1 sample are found as 3.88 wt. % and 13.10 wt. %, respectively. After EDTA-Na_2 was added into the electrolyte, Ca= 8.87 wt. % and P=14.61 w.t % in B2 sample, Ca= 7.76 wt. % and P=13.10 wt. % in B3 sample and Ca= 6.96 wt. % and P=13.71 wt. % in B4 sample. The ratio of Ca and P elements on the coating surfaces is Ca/P B1= 0.29, B2= 0.60, B3= 0.54, and B4= 0.50. After the MAO process, by adding EDTA-Na_2 into the electrolyte, it is seen that there is more Ca element on the coating surfaces compared to B1. Here, it is understood that EDTA-Na_2 is an agent that ensures more Ca ions on the coating surface. It was understood that the increase in the Ca element on the coating surface in B2, B3, and B4, shown in Fig. 3, caused the deterioration of the sphericity of the pores.

Fig. 5 shows the applied voltage during the MAO process for all samples. It can be seen that the MAO process has three stages, as mentioned above. During the first stage, the voltage linearly increases at a constant rate over time. At this stage (0 - 200V), firstly, the Ti6Al4V alloy substrate dissolves and notably decreases its metal brightness, afterward, a thin coating layer is formed on the anode surface [18]. When the voltage surpasses a critical value (325 V), many small micro-sparks can be observed on the sample surfaces. The critical voltage is described as the breakdown voltage and is related to the appearance of micro-sparks on the sample surface. Electrolytic composition and conductivity are strongly related to breakdown voltage [19].

XRD Analysis

X-ray diffraction patterns of the MAO-treated samples (B1, B2, B3, and B4) are shown in Fig. 6, which indicate the phase composition of the coating consisting of Ti and TiO_2 allotropes (Anatase and/or Rutile phase). Anatase is a metastable phase, while the rutile phase is a stable phase [20]. In the phase composition of sample B1, only the anatase phase was detected on the coating surface after the MAO treatment conducted without the addition of EDTA-Na_2 to the electrolyte. Similarly, in sample B2, the coating surface exhibited only the anatase phase following the addition of EDTA-Na_2 to the electrolyte. However, in samples B3 and B4, an increase in the amount of EDTA-Na_2 in the electrolyte during the MAO process led to the transformation of the anatase phase into the rutile phase. In sample B4, the rutile phase seemed to be more distinguishable. While the XRD peaks of the anatase phase were found at 25.30° (011) and 48.14° (020), the rutile phases were found at 27.35° (110) and 36.13° (101). It has not been determined what the peaks at 22.15° and 24.63° belong to. At the early phase of the MAO treatment, reactions between Ti^{4+} and OH^- ions in the microdischarge channels result in the development of anatase and rutile structures on the surface. As the processing time increases, anatase turns into rutile as a result of the increase in temperature in the micro-discharge channels. The temperature of the anatase transformation to rutile is approximately 953 K. [21]. The local temperature in microdischarge channels varies from 800–3000 to 10,000–20,000 K during the MAO process [22]. In the B3 and B4 samples, the rutile phase formed at high temperatures was obtained by the addition of EDTA-Na_2 to the electrolyte. This phenomenon can be explained by the increase in the temperature of discharge channels in electrolytes containing EDTA-Na_2. A combination of anatase and rutile phases is desirable in the coating layer because it enhances cell proliferation and accelerates osseointegration between the implant and surrounding tissue. [20].

The anodic oxidation process of Ti can be represented by the following equations [23,24];

$$Ti \rightarrow Ti^{4+} + 4e^- \quad (1)$$
$$Ti + 4OH^- \rightarrow TiO_2 + 2H_2O \quad (2)$$
$$Ti + 2H_2O \rightarrow TiO_2 + 4H^+ \quad (3)$$
$$Ti + 1/2\ O_2 \xrightarrow{610\ °C} TiO_2\ (Anatase) \xrightarrow{730\ °C} TiO_2\ (Rutile) \quad (4)$$

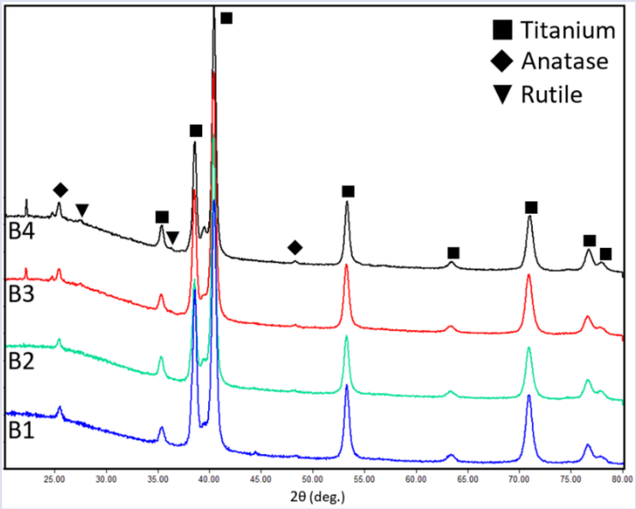

Figure 6. XRD analysis of B1, B2, B3, and B4 after MAO treatment.

Pore Size

The average pore size was calculated by measuring the diameter of pores using SEM images of MAO-treated samples B1, B2, B3, and B4. The average pore size of the samples is calculated using ImageJ quantitative image analysis software and presented in Table 3. For each sample, 80 pores were measured and the average value was calculated. After the MAO process, without the addition of EDTA-Na_2 into the electrolyte, the average pore size is calculated approximately 1 µm (B1). Subsequently, the addition of EDTA-Na_2 to the electrolyte during the MAO process led to an increase in pore size (B2), whereas further increasing the EDTA-Na_2 concentration resulted in a decrease in pore size (B3 and B4) due to the phenomenon of "pore coalescence." It has been reported that EDTA-Na_2 changes the pore sizes and is related to the intensity of micro-discharges. [25] A higher electrolyte concentration in the solution lead to the release of more ions into the coating, enhancing its conductivity and subsequently reducing micro-arc spark discharges on the surface [26]. In conclusion, varying the amount of EDTA-Na_2 added to the electrolyte influences the pore size, which means it can be used to control the pore size.

Table 3. The average pore size of B1, B2, B3, and B4 was produced by the MAO process.

Sample Name	B1	B2	B3	B4
Average Pore Size (µm)	1,032 ± 0,3	2,420 ± 0,7	2,316 ± 0,7	2,130 ±0,7

Table 4. Average surface roughness of coating surfaces and uncoated Ti6Al4V.

Sample Name	1. area (µm)	2. area (µm)	3. area (µm)	Mean (µm)
Untreated Ti6Al4V	0,218	0,111	0,139	0,156 ± 0,056
B1	0,444	0,491	0,472	0,469 ± 0,024
B2	0,555	0,523	0,525	0,534 ± 0,018
B3	0,523	0,512	0,512	0,516 ± 0,006
B4	0,496	0,510	0,517	0,507 ± 0,011

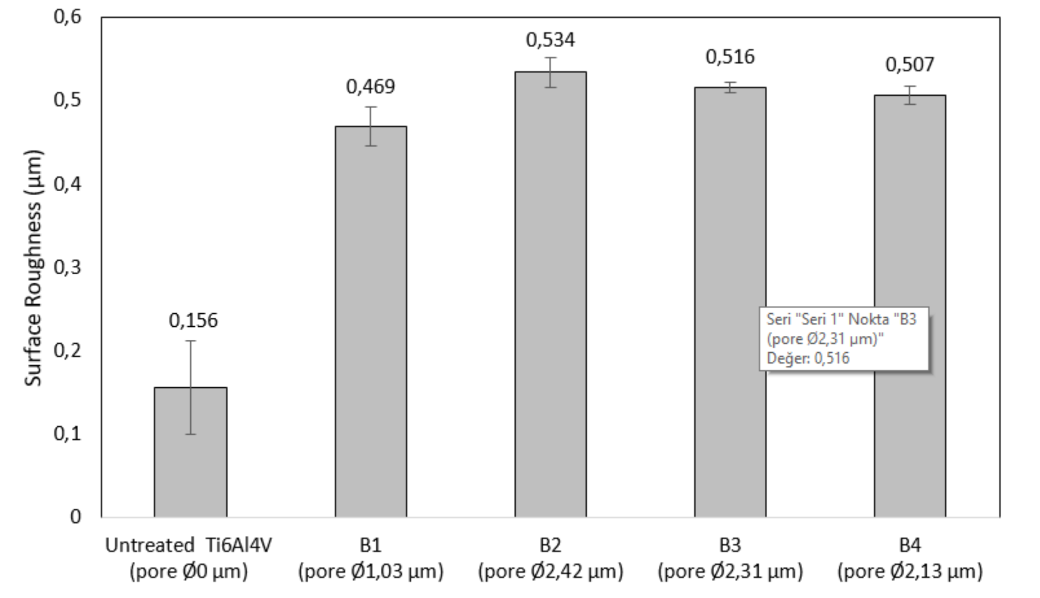

Figure 7. Surface roughness of MAO treated and untreated samples.

Surface Roughness

The surface roughness of untreated Ti6Al4V alloy and MAO-treated samples is presented in Table 4. For each sample, surface roughness were measured at three different points on the surface, and the average value was calculated. The *Ra* factors of the MAO layers are significantly higher than the untreated Ti6Al4V. Fig. 7 presents roughness values of MAO-treated and uncoated Ti6Al4V alloy against pore size. It is evident that pore size has a significant influence on surface roughness. The application of the MAO process to the untreated Ti6Al4V alloy resulted in a threefold increase in surface roughness. As the pore size increased (sample B2), a slight increase in surface roughness was observed, whereas a reduction in pore size (samples B3 and B4) led to a slight decrease in surface roughness. In literature, it is reported that the formation of pores is known to induce changes in the roughness of the coating [25].

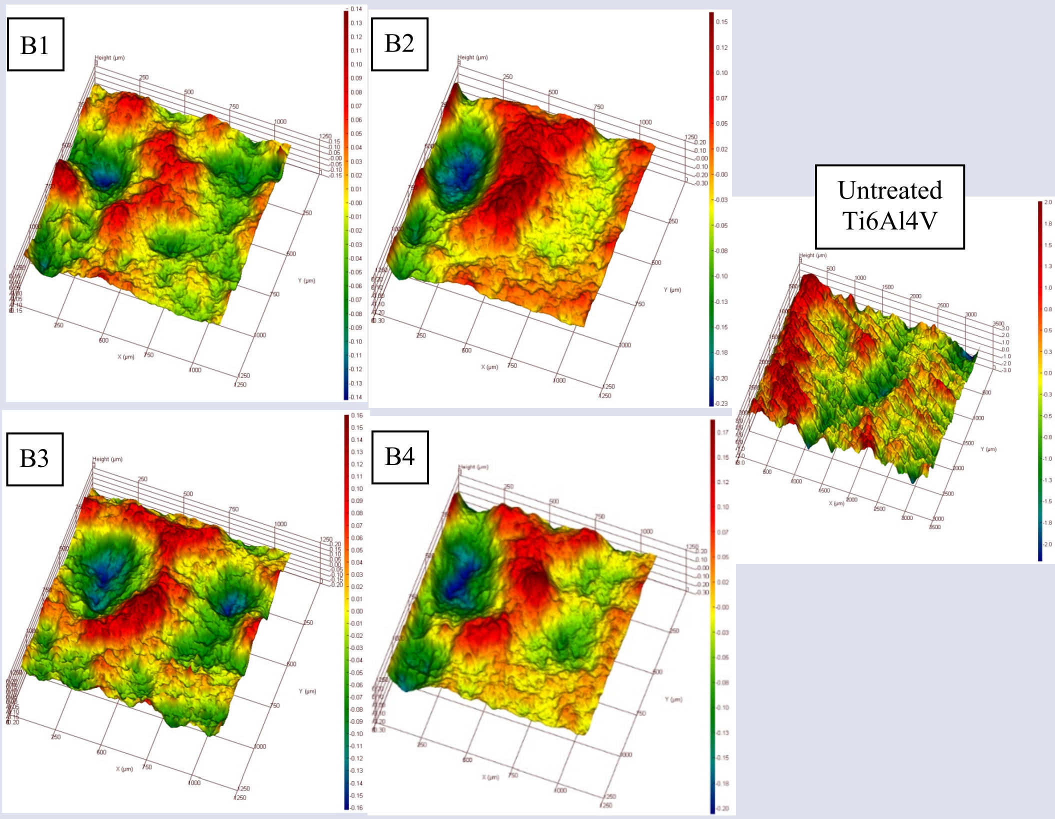

Figure 8. 3D AFM images of the untreated Ti6Al4V and the MAO-treated samples (B1, B2, B3, and B4).

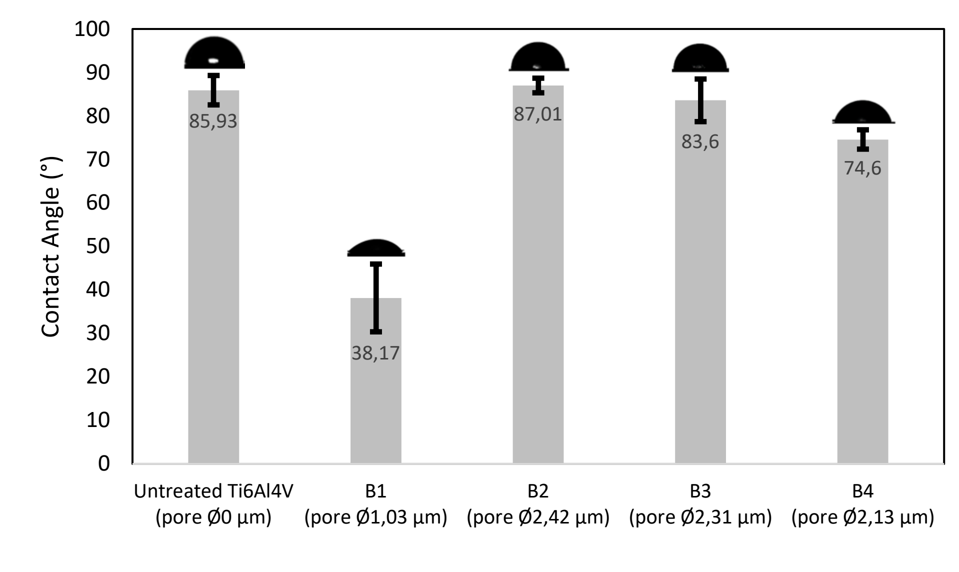

Figure 9. Contact angle of untreated Ti6Al4V and MAO-treated samples with varying EDTA-Na_2 additions in the electrolyte.

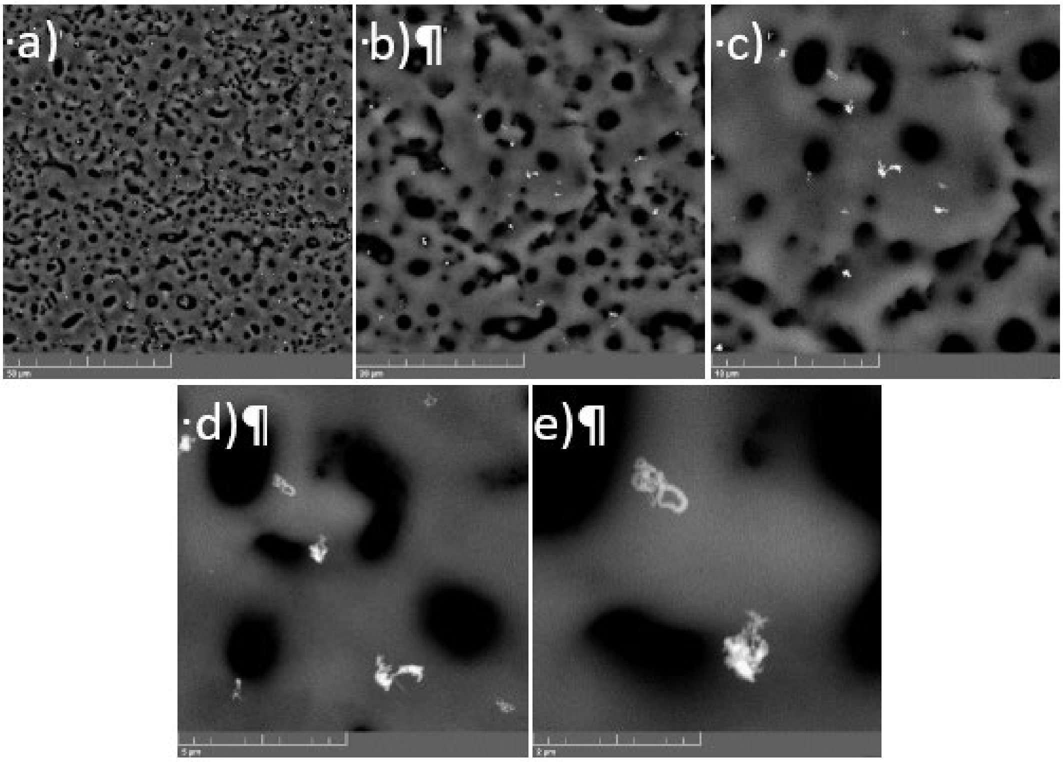

Figure 10. SEM images of AgNs obtained in the solution consisting of 100 mg $AgNO_3$ and 100 mg $C_6H_{12}O_6{\cdot}H_2O$ with UV irradiation method at various magnification a) 2 kX, b) 5 kX, c) 10 kX, d) 20 kX, e) 50 kX.

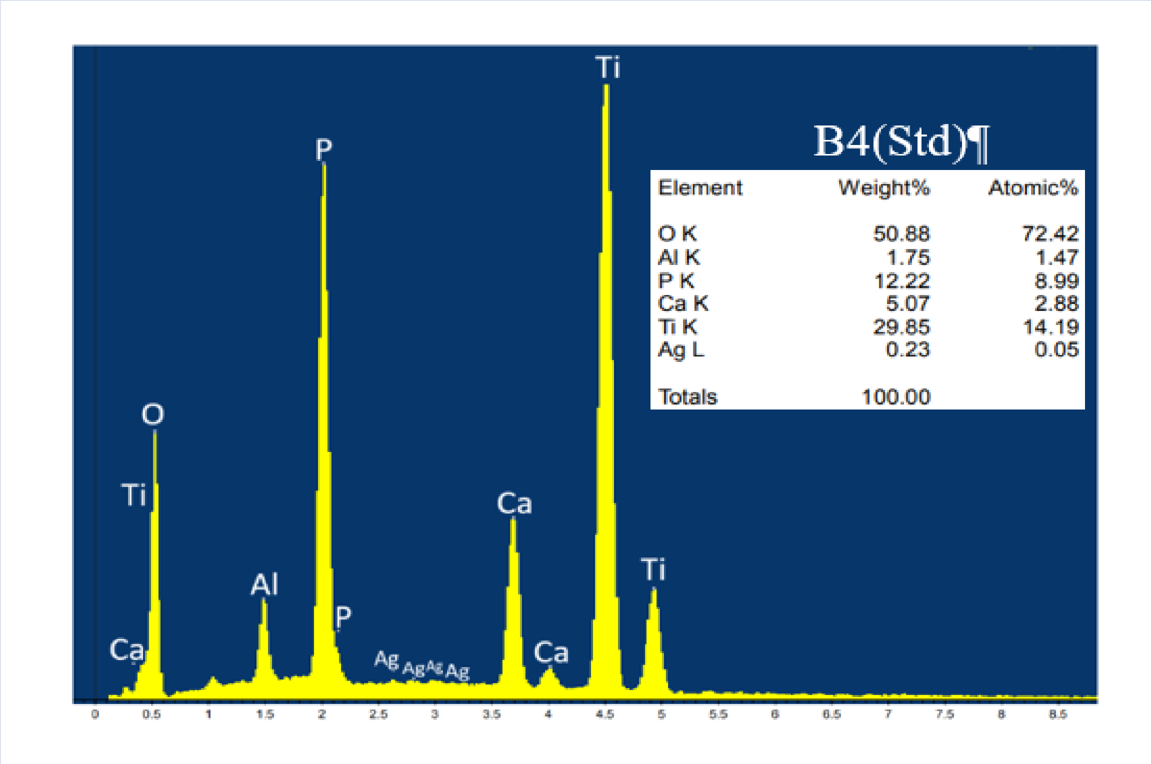

Figure 11. EDS analysis of B4(Std) sample.

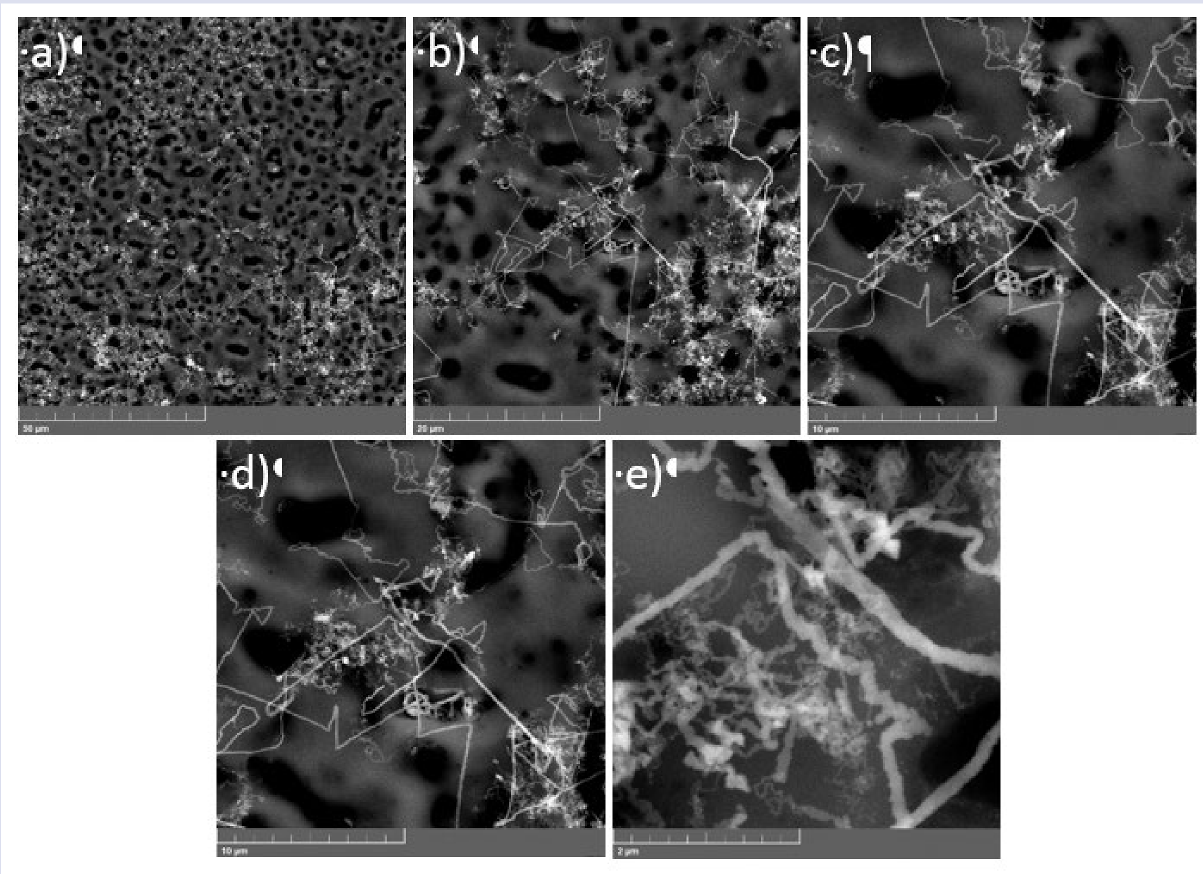

Figure 12. SEM images of AgNs obtained in the solution consisting of 1 g $AgNO_3$ and 1 g $C_6H_{12}O_6 \cdot H_2O$ at various magnifications: a) 2 kX, b) 5 kX, c) 10 kX, d) 20 kX, e) 50 kX.

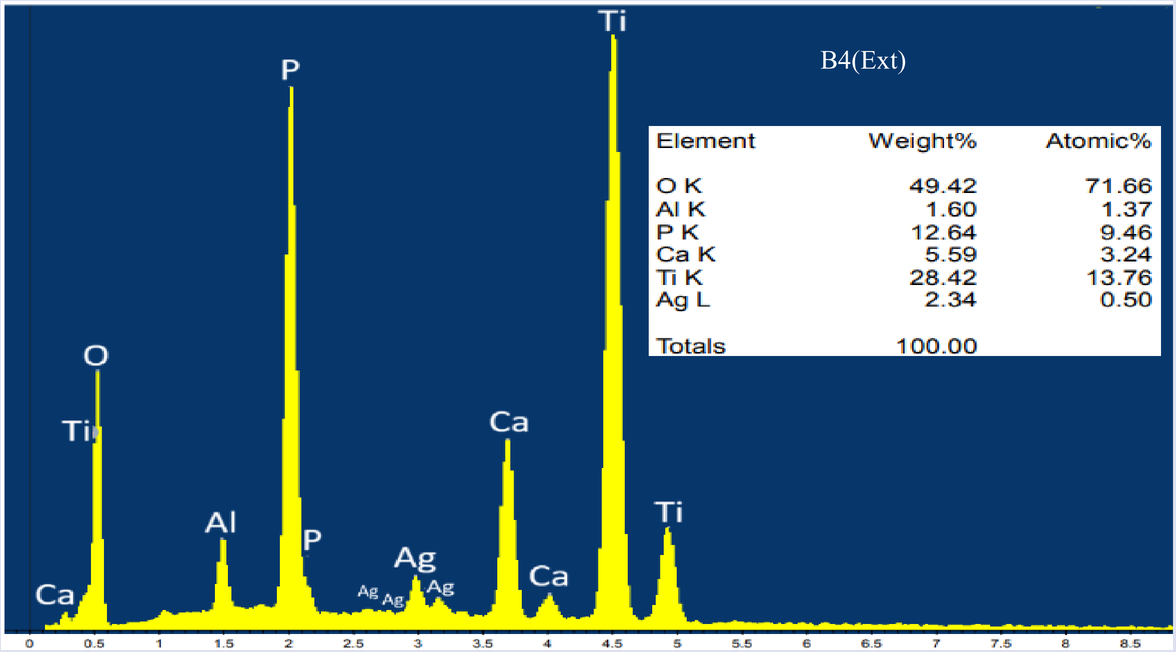

Figure 13. EDS analysis of B4(Ext) sample.

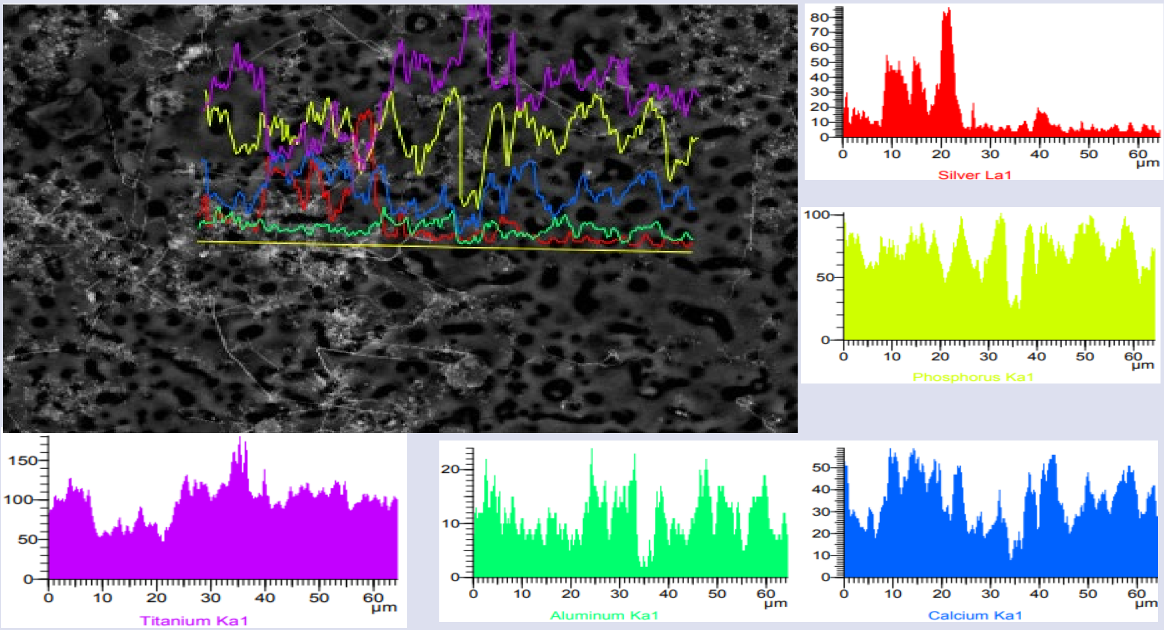

Figure 13. EDS analysis of B4(Ext) sample.

Wettability

Wettability is a notable property of biomaterials and cell adhesion, generally better on hydrophilic surfaces [29]. The contact angle is an important parameter used to assess the wettability of a material's surface. For better wettability, lower contact angles are needed. If the contact angle is lower than 90°, the surfaces are defined as hydrophilic, and if it is above 90°, the surfaces are defined as hydrophobic [30]. For each sample, contact angles were measured at three different points on the surface, and the average value was calculated. Fig. 9 shows the contact angles of untreated Ti6Al4V and MAO-treated samples, and it can be seen that the surfaces of all MAO-treated samples are wettable. While the MAO treatment without EDTA-Na_2 (B1) led to a significant decrease in the contact angle of the sample, the addition of EDTA-Na_2 to the electrolyte (B2) caused a significant increase in the contact angle. Increasing the amount of EDTA-Na_2 added to the electrolyte led to a slight decrease in the contact angle after the MAO treatment (B3, B4). It can be seen that the EDTA-Na_2 affects the surface wettability. It is also thought that EDTA-Na_2 increases surface energy. In literature, it is reported that contact angles are related to the surface energy of solids. As the surface energy of a solid increases, its wettability increases, resulting in a lower contact angle [31]. According to Fig. 8, it can be observed that there is a correlation between pore size and wettability among MAO-treated samples. As the pore size increases, the wettability of the coating surface decreases, and as the pore size decreases, it increases among MAO-treated samples.

Silver Nanostructure (AgNs) Deposition

For AgNPs deposition, sample B4 was selected based on its surface roughness, wettability, and phase composition. Two sets of deposition conditions were applied, with the samples referred to as B4(std) for standard conditions and B4(ext) for extreme conditions.

Fig. 10 SEM images indicate the AgNs produced on the B4 surface using the UV irradiation method under standard conditions, prepared with a solution consisting of 100 mg $AgNO_3$ and 100 mg $C_6H_{12}O_6{\cdot}H_2O$ mixture. AgNs are homogeneously dispersed across the surface. It can be observed that the produced AgNs appear thread-like and grain-like. The average thickness of the thread-like AgNs is 77 nm, while the average diameter of the grain-like AgNs is 65 nm. Fig. 10 indicates the EDS analysis of AgNs on the B4(std) surface produced under UV irradiation. According to the EDS analysis of the B4(std) sample, it is confirmed that silver is present on the MAO layer (Fig. 11).

Fig. 12 shows the SEM images of AgNs produced on the B4 surface under UV irradiation method at extreme conditions, prepared with a solution consisting of 1 g $AgNO_3$ and 1 g glucose monohydrate ($C_6H_{12}O_6{\cdot}H_2O$) mixture. It can be observed that the thread-like AgNs in Fig. 12 exhibit greater length and thickness compared to those in Figure 10. In other words, it has been understood that AgNs aggregate under extreme conditions and form a thread-like structure. The average thickness of the thread-like AgNs increased to 150 nm. These thread-like AgNs are homogenously dispersed onto the B4(Ext) sample after UV irradiation. It is observed that these thread-like AgNs wrap the MAO surface like a spider's web, suggesting that they may strongly adhere to the surface, as the contact area between the MAO-treated surface and the thread-like AgNs is large.

Fig. 13 shows the EDS analysis of sample B4(Ext). EDS analysis confirmed that silver is present on the MAO-treated surface. Increasing $AgNO_3$ concentration, increasing UV irradiation time, and decreasing the distance between the sample and UV lamps increased AgNs deposition. The line mapping evaluation performed on the MAO-treated surface is shown in Fig. 14. A straight line was drawn from left to right to show that the thread-like structure formed is silver. Silver peaks are observed in regions where there is a threadlike structure, while silver peaks are not observed in regions where there is no thread-like structure. To the best of our knowledge, AgNs deposition on a MAO-treated surface under UV irradiation is the first in the literature. Additionally, this type of AgNs has not been encountered in the literature in terms of its shape.

Ion Release

In this research, the ion release behavior of silver ions was analyzed in the SBF solution. SBF is prepared by dissolving the reagent listed in Table 5. This list was prepared according to Kokubo's recipe [32]. A 1000 mL glass bottle was filled with 700 mL ultra-pure water. The bottle was put on a magnetic stirrer with a heater. A thermometer and pH meter were inserted into the bottle. Reagents of 1st to 8th were dissolved at 36,5±1,5 ^oC one by one in the order shown in Table 3. After that, the 9th reagent (Tris) was dissolved gradually to avoid local pH increments. When the pH value of the solution reached 7,45, it was reduced to 7,42 by dropping HCl. When the total amount of Tris was finished, HCl was added to the solution until the pH value reached 7.40. After all, pure water was added to the solution until 1000 mL. For measuring ion release, the sample B4(Ext) was selected. Fig. 15 shows the variations of Ag ion concentrations in the SBF solution against immersion time. Also, titanium and vanadium ion release was investigated in the SBF solution. Silver ion release gradually decreased on the 1st, 3rd, and 5th days according to Fig. 14. The minimum silver concentration for the antimicrobial effect should be higher than 0,1 ppb, and the maximum toxic concentration for human cells should be lower than 10 ppm [33]. Accordingly, the total silver ion concentration obtained at the end of the 5th day is at an amount that can create some toxic effects. This is because the surface area of the thread-like silver structure is high, and the $AgNO_3$ concentration formed in the UV irradiation process under extreme conditions is high. The toxic effect can be reduced by reducing the $AgNO_3$ concentration. In addition, using a sample with a lower surface area will also reduce the toxicity because less AgNs will accumulate on the surface of a sample with a lower surface area. In addition, titanium and vanadium ions exhibited relatively stable but slightly elevated levels throughout the immersion period, which may reflect minor dissolution from the underlying alloy or partially soluble oxide regions.

Table 5. The reagent list used for SBF preparation

Reagent	Amount (g/L)
1- NaCl	8,035
2- $NaHCO_3$	0,355
3- KCl	0,225
4- $K_2HPO_4.3H_2O$	0,231
5- $MgCl_2.6H_2O$	0,311
6- 1M HCl	39 mL
7- $CaCl_2$	0,292
8- Na_2SO_4	0,072
9- Tris	6,118
10- 1M HCl	0-5 mL

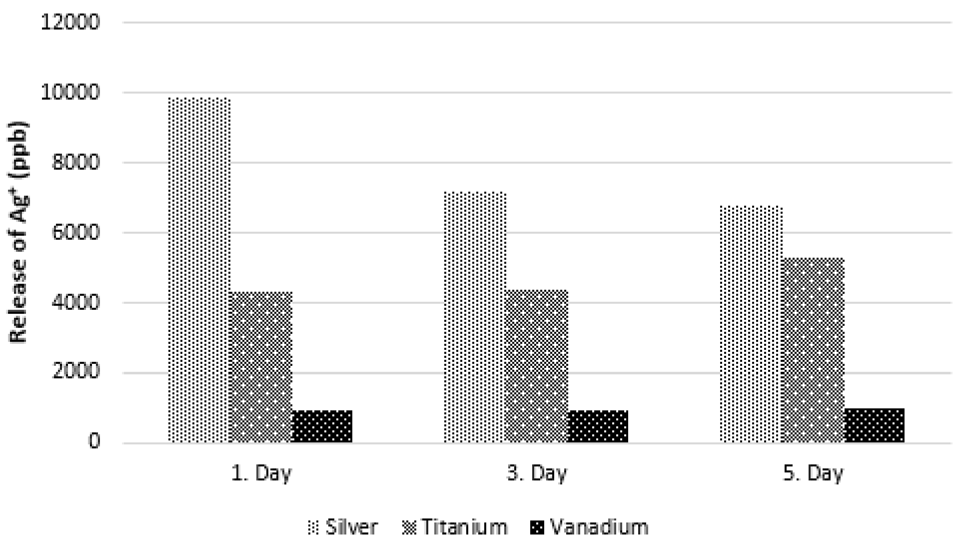

Ion	Silver (ppb)	Titanium (ppb)	Vanadium (ppb)
1. Day	8879	4341	912
3. Day	7198	4362	960
5. Day	6785	5295	975

Figure 15. Ion release of the sample B4(Ext) at 1st, 3rd and 5th day.

Conclusions

MAO treatment was successfully performed on Ti6Al4V alloy. EDTA-Na_2 created an effect in morphology in the MAO treatment. While the pores in sample B1 showed sphericity, in samples B2, B3, and B4, two or more pores merged and deviated from sphericity. According to EDS analysis, elements dissolved in the electrolyte passed to the coating surface, and EDTA-Na_2 provided Ca elements to be contained more on the coating surface. According to XRD analysis, EDTA-Na_2 had a positive effect on phase composition, and it also provided the formation of the rutile phase in B3 and B4 samples. Different amounts of EDTA-Na_2 caused changes in pore diameters. Here, EDTA-Na_2 acted as an agent controlling pore diameters as well as phase composition. It was found that surface roughness varies in direct proportion to pore diameter. Surface roughness increased with increasing pore diameter, while surface roughness decreased with decreasing pore diameter. Surface roughness changed in direct proportion to pore diameter. There is an inversely proportional relationship between pore diameter and wettability in MAO-treated samples. Although EDTA-Na_2 slightly reduced the wettability of the samples (B2, B3, B4), all MAO-treated surfaces showed wettability.

In the AgNs deposition process performed with the UV-A irradiation method, nanoparticles have a thread-like appearance. Due to their large surface area, thread-like structures are expected to exhibit a larger contact area with the underlying surface. Therefore, it is thought that their ability to adhere to the surface is also high. In the ion release experiment, it was observed that they released silver ions for a long time. The released silver ion is at a somewhat toxic level. The toxicity can be eliminated by reducing the amount of AgNs deposited on the surface. This type of AgNs has the potential to kill bacteria. As previously reported, silver functions as an antibacterial agent. A previous study reported the deposition of silver nanostructures within TiO_2 nanotubes via a UV-irradiation method, which demonstrated antibacterial activity against *E. coli* and *S. aureus* [15]. To the best of our knowledge, a similar structure has not been encountered in the literature, and the process of silver deposition using UV irradiation method on the surface of samples after MAO treatment of Ti6Al4V was the first in the literature. Deposition of silver on the surface by UV radiation is an effective technique that stands out with its low cost. This method does not require any complex equipment and can be performed at room temperature, significantly reducing energy and equipment costs. In addition, this process, which is carried out in a closed environment, makes the process both environmentally friendly and economical.

Acknowledgement

This work is supported by the Scientific Research Project Fund of Sivas Cumhuriyet University under the project number M-2024-863.

Conflicts of Interest

There is no conflicts of interest in this work.

References

[1] Geetha, M.B., Singh, A.K., Asokamani, R., & Gogia, A.K. (2009). Ti based biomaterials, the ultimate choice for orthopaedic implants – A review. *Progress in Materials Science, 54*, 397-425.

[2] Leyens, C., & Peters, M. (Eds.). (2006). Titanium and titanium alloys: fundamentals and applications. Wiley-vch.

[3] Brunette, D. M., Tengvall, P., Textor, M., & Thomsen, P. (2001). Titanium in medicine: material science, surface science, engineering, biological responses and medical applications (p. 232). Berlin: Springer.

[4] Yerokhin, A., Nie, X.K., Leyland, A., & Matthews, A. (2000). Characterisation of oxide films produced by plasma electrolytic oxidation of a Ti–6Al–4V alloy. *Surface & Coatings Technology, 130*, 195-206.

[5] Wang, J., Pan, Y., Feng, R., Cui, H.W., Gong, B., Zhang, L., Gao, Z., Cui, X., Zhang, H., & Jia, Z. (2020). Effect of electrolyte composition on the microstructure and bio-corrosion behavior of micro-arc oxidized coatings on biomedical Ti6Al4V alloy. *Journal of Materials Research and Technology*.

[6] Han, Y., & Xu, K. (2004). Photoexcited formation of bone apatite-like coatings on micro-arc oxidized titanium. *Journal of biomedical materials research. Part A, 71 4*, 608-14.

[7] Song, W., Jun, Y., Han, Y., & Hong, S. (2004). Biomimetic apatite coatings on micro-arc oxidized titania. *Biomaterials, 25 17*, 3341-9.

[8] Chen, J., Shi, Y., Wang, L., Yan, F., & Zhang, F. (2006). Preparation and properties of hydroxyapatite-containing titania coating by micro-arc oxidation. *Materials Letters, 60*, 2538-2543.

[9] Yerokhin, A., Nie, X., Leyland, A., Matthews, A., & Dowey, S. (1999). Plasma electrolysis for surface engineering. *Surface & Coatings Technology, 122*, 73-93.

[10] Durdu, S., & Usta, M. (2012). Characterization and mechanical properties of coatings on magnesium by micro arc oxidation. *Applied Surface Science, 261*, 774-782.

[11] Durdu, S., Aytaç, A., & Usta, M. (2011). Characterization and corrosion behavior of ceramic coating on magnesium by micro-arc oxidation. *Journal of Alloys and Compounds, 509*, 8601-8606.

[12] Durdu, S., Deniz, Ö., Kutbay, I., & Usta, M. (2013). Characterization and formation of hydroxyapatite on Ti6Al4V coated by plasma electrolytic oxidation. *Journal of Alloys and Compounds, 551*, 422-429.

[13] Gabor, R., Doubková, M., Gorosova, S., Malaník, K., Vandrovcová, M., Cvrček, L., Drobikova, K., Mamulová Kutláková, K., & Bačáková, L. (2020). Preparation of highly wettable coatings on Ti–6Al–4V ELI alloy for traumatological implants using micro-arc oxidation in an alkaline electrolyte. *Scientific Reports, 10*.

[14] Durdu, S., Aktug, S.L., Korkmaz, K., Yalçın, E., & Aktaş, S. (2018). Fabrication, characterization and in vitro properties of silver-incorporated TiO2 coatings on titanium by thermal evaporation and micro-arc oxidation. *Surface and Coatings Technology*.

[15] Zhao, C., Feng, B., Li, Y., Tan, J., Lu, X., & Weng, J. (2013). Preparation and antibacterial activity of titanium nanotubes loaded with Ag nanoparticles in the dark and under the UV light. *Applied Surface Science, 280*, 8-14.

[16] Rheima, A.M., Mohammed, M.A., Jaber, S.H., & Hameed, S.A. (2019). Synthesis of Silver Nanoparticles Using the UV-Irradiation Technique in an Antibacterial Application. *Journal of Southwest Jiaotong University*.

[17] Echeverry-Rendón, M., Galvis, O., Quintero Giraldo, D., Pavón, J.J., López-Lacomba, J.L., Jiménez-Piqué, E., Anglada, M., Robledo, S.M., Castaño, J.G., & Echeverría, F.E. (2015). Osseointegration improvement by plasma electrolytic oxidation of modified titanium alloys surfaces. *Journal of Materials Science: Materials in Medicine, 26*, 1-18.

[18] Snizhko, L.O., Yerokhin, A., Pilkington, A., Gurevina, N.L., Misnyankin, D.O., Leyland, A., & Matthews, A. (2004). Anodic processes in plasma electrolytic oxidation of aluminium in alkaline solutions. *Electrochimica Acta, 49*, 2085-2095.

[19] Liang, J., Hu, L., & Hao, J. (2007). Characterization of microarc oxidation coatings formed on AM60B magnesium alloy in silicate and phosphate electrolytes. *Applied Surface Science, 253*, 4490-4496.

[20] Makurat-Kasprolewicz, B., & Ossowska, A. (2023). Recent advances in electrochemically surface treated titanium and its alloys for biomedical applications: A review of anodic and plasma electrolytic oxidation methods. *Materials Today Communications*.

[21] Okada, K., Yamamoto, N., Kameshima, Y., Yasumori, A., & MacKenzie, K. (2004). Effect of Silica Additive on the Anatase-to-Rutile Phase Transition. *Journal of the American Ceramic Society, 84*, 1591-1596.

[22] Yerokhin, A., Nie, X., Leyland, A., Matthews, A., & Dowey, S. (1999). Plasma electrolysis for surface engineering. *Surface & Coatings Technology, 122*, 73-93.

[23] Yerokhin, A., Parfenov, E.V., & Matthews, A. (2016). In situ impedance spectroscopy of the plasma electrolytic oxidation process for deposition of Ca- and P-containing coatings on Ti. *Surface & Coatings Technology, 301*, 54-62.

[24] Sun, M., Jiang, M., Huang, H., Yang, B., Lin, Y., & Wang, P. (2023). Effect of HfO_2 Particles on Ceramic Coating Fabricated on Ti6Al4V Alloy via Plasma Electrolytic Oxidation. *Coatings*, *13*(5), 967.

[25] Ríos, J. M., Quintero, D., Castaño, J. G., Echeverría, F., & Gómez, M. A. (2022). Effect of EDTA addition on the biotribological properties of coatings obtained from PEO on the Ti6Al4V alloy in a phosphate-based solution. *Surfaces and Interfaces*, *30*, 101857.

[26] Adeleke, S.A., Bushroa, A.R., & Sopyan, I. (2017). Characteristic Features of Plasma Electrolytic Treated Layers in Na3PO4 Solution. *Procedia Engineering, 184*, 732-736.

[27] Albrektsson, T., & Wennerberg, A. (2004). Oral implant surfaces: Part 1--review focusing on topographic and chemical properties of different surfaces and in vivo responses to them. *The International journal of prosthodontics, 17(5)*, 536-43.

[28] Yang, Z., Xia, L., Sun, W., & Li, W.J. (2011). Effect of Surface Characteristics on Bioactivity of Ceramic Coating on Ti6al4v by Plasma Electrolytic Oxidation. *Advanced Materials Research, 320*, 33 - 37.

[29] Cao, H., & Liu, X. (2013). Activating titanium oxide coatings for orthopedic implants. *Surface & Coatings Technology, 233*, 57-64.

[30] Rupp, F., Gittens, R.A., Scheideler, L., Marmur, A., Boyan, B.D., Schwartz, Z., & Geis-Gerstorfer, J. (2014). A review on the wettability of dental implant surfaces I: theoretical and experimental aspects. *Acta biomaterialia, 10 7*, 2894-906.

[31] Hsieh, C., Tsai, S., Wang, D., Chang, Y., & Hsieh, H. (2005). Preparation of gamma-PGA/chitosan composite tissue engineering matrices. *Biomaterials, 26 28*, 5617-23.

[32] Kokubo, T., & Takadama, H. (2006). How useful is SBF in predicting in vivo bone bioactivity? *Biomaterials, 27 15*, 2907-15.

[33] Jamuna-Thevi, K., Bakar, S.A., Ibrahim, S., Shahab, N., & Toff, M.R. (2011). Quantification of silver ion release, in vitro cytotoxicity and antibacterial properties of nanostuctured Ag doped TiO2 coatings on stainless steel deposited by RF magnetron sputtering. *Vacuum, 86*, 235-241.